Catalysis Today 158 (2010) 146–155

Contents lists available at ScienceDirect

Catalysis Today

journal homepage: www.elsevier.com/locate/cattod

Structural and vibrational properties of molybdena catalysts supported on alumina and zirconia studied by *in situ* Raman and FTIR spectroscopies combined with $^{18}O/^{16}O$ isotopic substitution

George Tsilomelekis, Soghomon Boghosian *

Department of Chemical Engineering, University of Patras and Institute of Chemical Engineering and High Temperature Chemical Processes, Foundation of Research and Technology – Hellas (FORTH/ICH-HT), GR-26500 Patras, Greece

ARTICLE INFO

Article history:
Available online 31 July 2010

Keywords:
Vibrational isotope effect
Oxygen-18
Raman spectra
IR spectra
Molybdena catalysts

ABSTRACT

Molybdena/alumina and molybdena/zirconia catalysts with Mo surface densities in the range 1.1–5.2 Mo/nm^2 were studied by *in situ* vibrational (Raman and FTIR) spectroscopies and $^{18}O/^{16}O$ isotopic exchange experiments combined with *in situ* Raman spectra at 450 °C. The vibrational isotope effects and the combined interpretation of Raman and IR band wavenumbers and characteristics suggest a mono-oxo configuration for the deposited molybdena phase on both catalytic systems at low (~1.5 Mo/nm^2) as well as at high (4–5 Mo/nm^2) coverage, irrespective of extent of association (polymerisation). Isolated mono-oxo monomolybdates predominate on alumina at low loadings, while increasing relative amounts of mono-oxo polymolybdates are formed at high loadings. Mono-oxo polymolybdates and monomolybdates occur on zirconia, with the polymolybdates predominating already from low coverage (1.7 Mo/nm^2). A "next-nearest-neighbor $^{18}O/^{16}O$ substitution" vibrational effect is observed, resulting in small red shifts (2–5 cm^{-1}) of the Mo=^{16}O Raman band wavenumber. The catalysts' behavior for the oxidative dehydrogenation of ethane is addressed and discussed with relevance to the configuration of deposited molybdena.

1. Introduction

Molybdena species [$(MoO_x)_n$] supported on oxide carriers constitute a class of interesting catalysts that are active for a number of processes including olefin metathesis [1], selective oxidation reactions [2,3], oxidative dehydrogenation (ODH) of light alkanes [4,5], the selective catalytic reduction of NO by NH_3 [6], etc. The surface composition, the local structure of the dispersed molybdena surface species, the active phase loading and the nature of the support are amongst important parameters that affect catalyst performance. The structure of supported molybdena catalysts at dehydrated conditions has been studied extensively, mainly by *in situ* Raman spectroscopy with most studies pertaining to alumina-supported catalysts [7]. The structure of the dispersed molybdena phase for coverages below monolayer evolves from isolated monomeric molybdates (MoO_x) to larger polymolybdates possessing Mo–O–Mo bridges [5,8]; at coverages exceeding the monolayer, crystalline MoO_3 or mixed metal oxide crystals (e.g. $Al_2(MoO_4)_3$ [8], $Zr(MoO_4)_2$ [5,9]) are formed. The occurrence of multiple Mo sites and the resulting heterogeneity of the dispersed molybdena phase renders the derivation of structure/function relationships quite challenging. On the other side, seen upon as a "good mix" or "favorable balance" of resulting properties, the structural and/or phase complexity of a catalyst may be advantageous in performance grounds for e.g. selective oxidation catalysts. Questions like e.g. whether the surface monomolybdate (abundant at low Mo surface densities) occurs in tetragonal pyramidal O=Mo(–O–*M*)$_4$, mono-oxo tetrahedral O=Mo(–O–*M*)$_3$ or di-oxo tetracoordinated (O=)$_2$Mo(–O–*M*)$_2$ (*M* = support metal atom) configuration are still open to a large extent and have been the subject of recent elegant theoretical (DFT) investigations for molybdena supported on silica and titania [10,11]. In particular, the group 5–7 transition metal oxides supported on SiO_2 have been the subject of a comprehensive investigation by *in situ* spectroscopic methods [12] including Raman work assisted with $^{18}O/^{16}O$ isotopic exchange experiments [13] and the results point undoubdetdly to an exclusive occurrence of dehydrated dispersed metal oxide species in isolated (monomeric) form. For the case of MoO_3/SiO_2 system, di-oxo (O=)$_2$Mo(–O–Si)$_2$ species prevail with small amounts of O=Mo(–O–Si)$_4$ also evidenced as being present [12,13]. However, the dispersion of supported metal oxide layers on SiO_2 has its own special character, being very low because of the low reactivity and greater acidic nature of the SiO_2 surface hydroxyls. To the contrary, more complex molecular structures are present in "non-SiO_2" sup-

* Corresponding author. Tel.: +30 2610 969557.
E-mail address: bogosian@iceht.forth.gr (S. Boghosian).

0920-5861/$ – see front matter © 2010 Elsevier B.V. All rights reserved.
doi:10.1016/j.cattod.2010.06.026

Table 1
Properties of the catalysts.

Catalyst	MoO_3 (wt%)	Calcination	Surface area (m^2/g)	Surface density n_s (Mo/nm^2)	Crystalline phases
2MoZr	2	600 °C/4 h	48.7	1.7	ZrO_2 (monoclinic)
5.5MoZr	5.5	600 °C/4 h	44.7	5.2	ZrO_2 (monoclinic)
5MoAl	4.8	650 °C/6 h	185.7	1.1	γ-Al_2O_3
15MoAl	14.8	650 °C/6 h	160.8	3.9	γ-Al_2O_3

ports (e.g. Al_2O_3, ZrO_2, TiO_2) where the dispersion is much higher and isolated metal oxide species coexist with polymeric domains.

In situ Raman spectroscopy is a valuable method for characterising supported metal oxide catalysts by probing the vibrational properties of metal–oxygen bonds [14,15]. Raman spectroscopy combined with IR spectroscopy and $^{18}O/^{16}O$ exchange experiments can shed light for the differentiation of mono-oxo and polyoxo deposited species [16,17]. The catalyst structure, however, is not static but responds to alterations in the catalyst/reactor environment [18]. The *operando* methodology [19,20] combining spectroscopic monitoring with simultaneous product analysis is a powerful upgraded approach for deriving structure/function relationships. Moreover, multi-operational spectroscopic reactor cells [21] used with a view to gain knowledge on spatiotemporal gradients in heterogeneous catalysts [22] constitute the new arsenal for deriving structure/function relationships. Such techniques can overcome obstacles which may relate *inter-alia* to site multiplicity and active phase heterogeneity (*i.e.* by taking spectra in several points).

Research aiming at the understanding of structural and vibrational properties of the dispersed phase of supported transition metal oxide catalysts is of topical character. The motivation of the present article, reporting on our pertinent endeavors on molybdena catalysts supported on zirconia and alumina, is threefold: (i) to differentiate between mono-oxo and di-oxo configurations for the deposited Mo(VI)–oxo species using *in situ* Raman and FTIR spectroscopies combined with $^{18}O/^{16}O$ isotopic substitution experiments; (ii) to examine spectroscopically the site/phase multiplicity at low (~1.5 Mo/nm^2) and medium-high (4–5 Mo/nm^2) Mo surface densities below monolayer coverage; and (iii) to exploit the vibrational isotope effects in order to study the reducibility of the various O sites (Mo=O, Mo–O–Mo and Mo–O-support). The results (building also on existing knowledge) contribute to the discussion on molecular structure and vibrational properties of deposited Mo(VI)–oxo species and address their possible relevance to catalyst behavior for the ODH of ethane.

2. Experimental

2.1. Catalyst preparation and characterisation

The catalysts were prepared by wet impregnation of the support materials [ZrO_2 (Norton, 55 m^2/g) and γ-Al_2O_3 (Engelhard, 183.9 m^2/g)] using aqueous solutions (pH = 4–5) of $(NH_4)_6Mo_7O_{24}{\cdot}4H_2O$ (Alfa). The solutions, of which the concentrations were adjusted so to correspond to the desired MoO_3 wt%, were subjected to rotation at 40–45 °C for 0.5–1 h and then to rotary evaporation at 45–70 °C under reduced pressure for 1.5 h in order to remove the solvent. Afterwards they were dried overnight at 100–140 °C and calcined in air in a muffle furnace (see Table 1 for details).

Surface areas were measured by N_2 adsorption using a Micromeritics Gemini II 2370 analyzer and standard multipoint BET analysis methods. Samples were evacuated for 2 h before N_2 adsorption measurements. Powder X-ray diffraction patterns were obtained at room temperature using a Philips PW 1830 diffractometer and CuKα radiation. The catalyst characteristics are summarised in Table 1. The samples are denoted by *x*Mo*M*, *x* being the wt% MoO_3 loading and *M* the support metal atom.

2.2. In situ Raman spectroscopy and $^{18}O/^{16}O$ exchange

A home made Raman cell was used for recording the *in situ* Raman spectra of the studied catalysts (Fig. 1) consisting of a

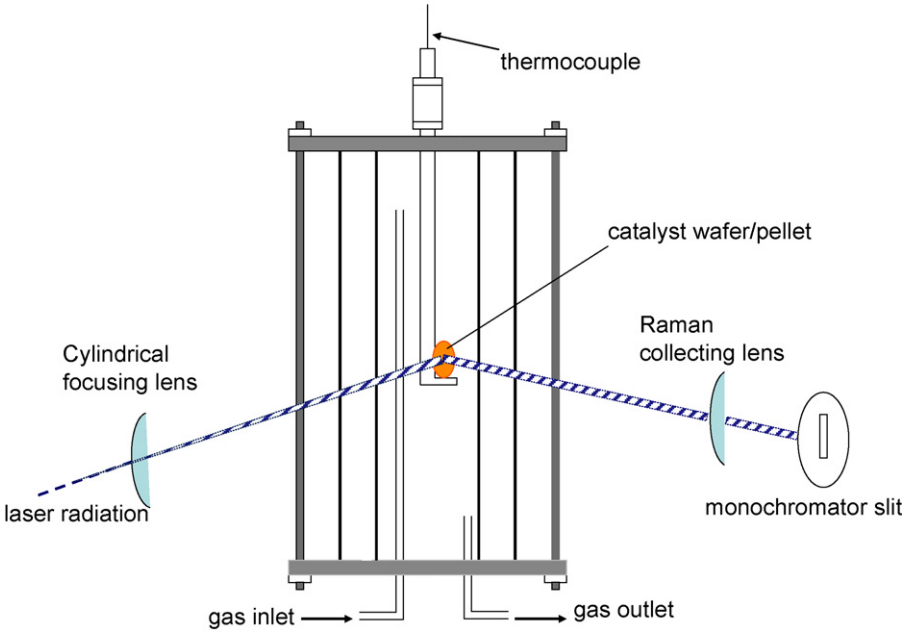

Fig. 1. Home-made *in situ* Raman cell.

double-walled quartz-glass transparent tube furnace mounted on a *xyz* plate allowing it to be positioned on the optical table. The inner furnace tube (23 mm o.d.; 20 mm i.d. and 10 cm long) is kanthal wire-wound for heating the cell. The cell has a gas inlet and a gas outlet as well as a thermocouple sheath possessing a sample holder at its tip. Approximately 180 mg of each catalyst were pressed into a wafer and mounted on the holder that could be vertically adjusted in the *in situ* cell.

The 488.0 nm line of a Spectra Physics Stabilite 2017 Ar^+ laser was used for exciting the Raman spectra of the studied catalysts. The incident light (adjusted approximately to 40 mW) was slightly defocused with a cylindrical lens in order to reduce sample irradiance. The scattered light was collected at 90° (horizontal scattering plane), analyzed with a 0.85 Spex 1403 double spectrometer and detected by a −20 °C cooled RCA PMT interfaced with a Labspec data acquisition software.

In situ Raman spectra under oxidising conditions were recorded at 450 °C under flowing $^{16}O_2$ (99.999%) after treatment for 1 h at a 15 cm^3/min flow rate. Afterwards, each catalyst was subjected to reducing conditions under flowing 4.5% H_2/N_2 for 15 min at a 50 cm^3/min flow rate and reoxidised with 2% $^{18}O_2$/He (Messer) for 15 min at a 10 cm^3/min flow rate. Intermittent *in situ* Raman spectra under flowing 2% $^{18}O_2$/He were then recorded. The reduction and reoxidation step durations were crucial, in order to ensure that reduction and reoxidation ($^{18}O/^{16}O$ exchange) take place to a satisfactory extent without waste of the expensive $^{18}O_2$. The reduction/reoxidation protocol was established by "simulating" the process using 2% $^{16}O_2$/He as the reoxidant. This simulation showed that a duration of 15 min for each step was capable for attaining 90% of the steady state in each cycle at 450 °C.

2.3. In situ FTIR spectroscopy

In situ Fourier transform infrared (FTIR) experiments were carried out under flowing $^{16}O_2$ at 450 °C using a Nicolet 740 FTIR spectrometer equipped with a diffuse reflectance (DRIFT) cell (Spectra Tech), an MCTB detector and a KBr beam splitter. The oxygen flow rate through the DRIFT cell was 30 cm^3/min.

2.4. Catalytic measurements

Catalytic measurements took place in a fixed-bed differential reactor operated at steady state ethane ODH conditions with a reactant gas feed consisting of 5.6% C_2H_6/5.6% O_2 balanced in He. Each catalyst sample was examined at a range of reactant residence times such that the reactor operation conditions could be considered as differential. The residence time is expressed in terms of the ratio W/F (W, catalyst weight in the range 150–350 mg; F, total gas flow in the range 20–200 cm^3/min). By varying either the catalyst weight or the total flow rate, the resulting W/F values ranged between 0.05 and 0.67 g s/cm^3. Before changing the operating temperature or the W/F ratio each sample was reoxidised under flowing O_2 at 550 °C in order to reinstate the initial oxidised catalyst state. All gas flow rates were controlled by electronic mass flow meters. The reactor effluent was analyzed by on-line GC (Schimadju 14B) using two packed columns (Porapak Q and Molecular Sieve 5A) in a series or bypass configuration and a thermal conductivity detector (TCD). Blank runs with no catalyst in bed were also performed in order to check the case of gas phase reaction contributions. Ethane conversion was less than 1% at 540 °C.

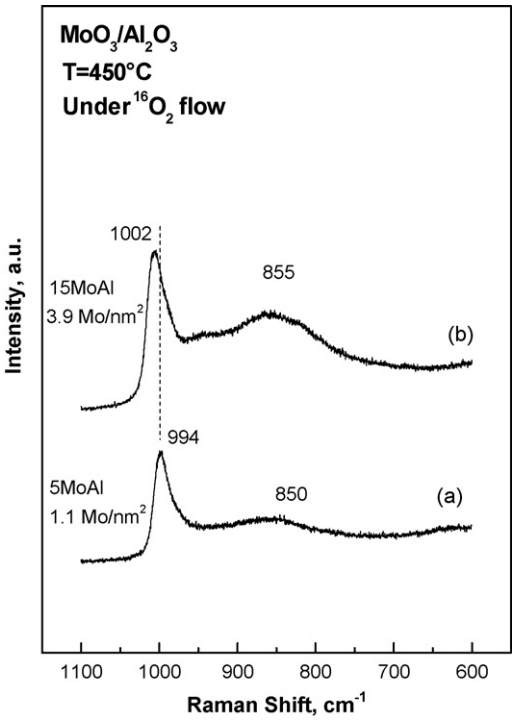

Fig. 2. *In situ* Raman spectra of oxidised MoO_3/Al_2O_3 catalysts under flowing $^{16}O_2$ at 450 °C: (a) 5MoAl and (b) 15MoAl. Laser wavelength, λ_0 = 488.0 nm; laser power, w = 40 mW; spectral slit width, ssw = 7 cm^{-1}

3. Results and discussion

3.1. In situ vibrational (Raman and FTIR) spectra of oxidised catalysts under flowing $^{16}O_2$(g)

3.1.1. In situ Raman spectra

Figs. 2 and 3 show the *in situ* Raman spectra of the studied MoO_3/Al_2O_3 and MoO_3/ZrO_2 catalysts. Molybdena species occur exclusively in the form of dispersed amorphous metal oxides, in conformity with the reported ~4–5 Mo/nm^2 molybdate saturation capacity on Al_2O_3 and ZrO_2 (as well as in several metal oxide supports) [9,23]. A prevalence of isolated (monomeric) molybdates is evidenced in Fig. 2(a) for 5MoAl (1.1 Mo/nm^2) with a well-defined Mo=O band at 994 cm^{-1} and a weak broad band at ~850 cm^{-1} due to Mo–O–Mo functionalities witnessing the low presence of associated (polymeric) molybdates. With increasing loading (*i.e.* for 15MoAl with 3.9 Mo/nm^2, Fig. 2(b)) the relative abundance of associated species (represented by the 855 cm^{-1} Mo–O–Mo band) is increased, whereas the Mo=O band location is blue shifted to 1002 cm^{-1}. The situation is quite similar (though slightly diversified) in Fig. 3 pertaining to MoO_3/ZrO_2 catalysts. Bands at ~1000 and 985 cm^{-1} are seen in the Mo=O region indicating the provenance from two distinct species, namely monomeric and polymeric molybdates, respectively. Here, for 2MoZr (with 1.7 Mo/nm^2, Fig. 3(a)) associated species possessing Mo–O–Mo bridges (band at 837 cm^{-1}) are present to a significant extent, contrary to the Al_2O_3-supported low-loaded sample (see Fig. 2(a)). With increasing loading (*i.e.* for 5.5MoZr with 5.2 Mo/nm^2, Fig. 3(b)) the polymolybdates dominate and the Mo=O and Mo–O–Mo bands exhibit higher relative intensities and are blue shifted to 995 and 851 cm^{-1}, respectively. The observed blue shifts with increasing loading (Figs. 2 and 3) have been attributed to polymolybdate domain growth [9]. Bands observed below ~750 cm^{-1} in Fig. 3 are due to the monoclinic ZrO_2 support. The spectral features observed in Figs. 2 and 3 are *mutatis mutandis* similar to those reported

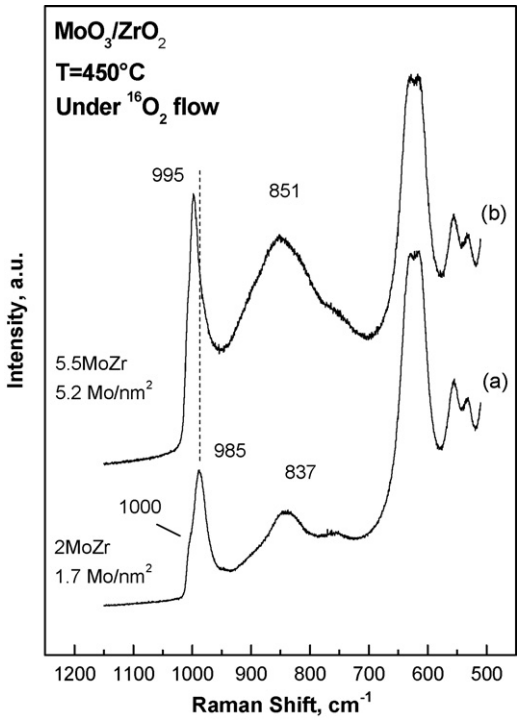

Fig. 3. *In situ* Raman spectra of oxidised MoO_3/ZrO_2 catalysts under flowing $^{16}O_2$ at 450 °C: (a) 2MoZr and (b) 5.5MoZr. Recording parameters: see Fig. 2 caption.

earlier by our group [5,8,24]. Notably, with increasing Mo surface density (up to ~7 Mo/nm^2) the intensity of the 800–900 cm^{-1} broad band assigned to Mo–O–Mo functionalities increases relative to the ~1000 cm^{-1} Mo=O band for both systems (*vide ante* Figs. 2 and 3 and Refs. [5,8,24]) thereby justifying the assignment of the broad band to Mo–O–Mo modes, because of the progressively (with increasing coverage) higher degree of association (polymerisation) that gives rise to a *higher number of Mo–O–Mo bridges relative to extant Mo=O sites*. If the broad band (here assigned to Mo–O–Mo) was e.g. due to Mo–O-support, then one would by no means expect an increase of its intensity relative to the Mo=O band. The assignment of the broad band to Mo–O–Mo functionalities is in agreement with the general consensus in catalysis literature [7,16,17,23,25–37]. However, this generally accepted view, which is in full conformity with the "coverage–dependent" Raman features (*vide ante* Figs. 2 and 3 and Refs. [5,8,24]) has recently been challenged for one case (VO_x on alumina) based on DFT calculations [38,39] by assigning a broad 945 cm^{-1} band to a V–O–Al mode of either a O=V(–O–Al)$_3$ or a O=V(–O–Al)$_4$ species.

At this point, it is worth making a comment with reference to the eventual diversifications in the literature-reported wavenumbers for *M*=O modes (*M* = transition metal) in *in situ* Raman studies of supported transition metal oxide catalysts, accounting also for the broadness exhibited by several bands. In dispersed amorphous metal oxides, the local structure exhibits certain symmetry, which reflects the bonding and the coordination around the transition metal atom. However, the local structure lacks periodicity, thereby giving rise to a distribution of related configurations resulting in site multiplicity and a broad character of the observed vibrational bands. The band broadness has an intrinsic character related to the existing distribution in bond lengths and strengths amongst related (but not identical) sites and is more pronounced for bridging rather than for terminal *M*–O functionalities.

3.1.2. *In situ* FTIR spectra and anharmonicity

Fig. 4 shows the *in situ* FTIR spectra of the studied catalysts in oxidised state under flowing $^{16}O_2$ at 450 °C. Unfortunately, only the overtone region can be exploited and in all cases shows one single band due to Mo=O at wavenumbers in the region 1950–1985 cm^{-1} (indicated by each spectrum and listed in Table 2). The band intensity appears to increase with increasing loading. Observing one single band in the IR overtone region is indicative of a mono-oxo configuration for the dispersed molybdena phase (*vide infra*, next Section 3.1.3 on structural implications). However, as seen in Table 2, the observed wavenumbers of the Mo=O overtones are not the same that would be predicted by doubling the corresponding

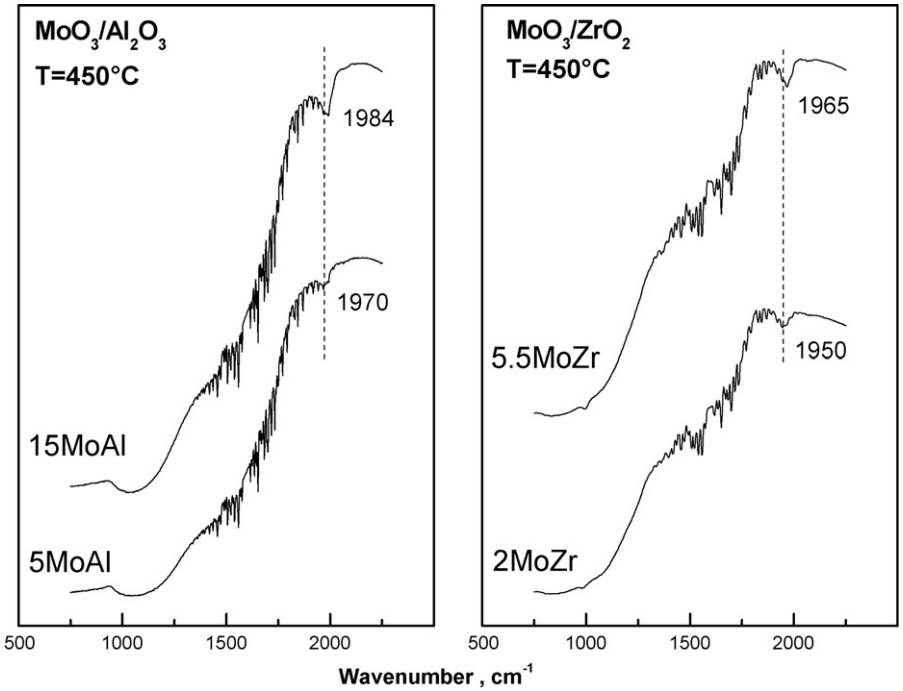

Fig. 4. *In situ* FTIR spectra of oxidised MoO_3/Al_2O_3 and MoO_3/ZrO_2 catalysts under flowing $^{16}O_2$ at 450 °C.

Table 2
Mo=O stretching modes for MoO_3/Al_2O_3 and MoO_3/ZrO_2 catalysts: observed Raman fundamentals ($\nu_{R,1\leftarrow0}$) and IR first overtones ($\nu_{IR,2\leftarrow0}$), calculated *zero-order* wavenumbers ($\omega_{Mo=O}$, corrected for anharmonicity[a]) and anharmonic constants ($x_{Mo=O}$[a]).

	5MoAl (1.7 Mo/nm^2)	15MoAl (3.9 Mo/nm^2)	2MoZr (1.1 Mo/nm^2)	5.5MoZr (5.2 Mo/nm^2)
$\nu_{Mo=O,1\leftarrow0}$ (Raman)/cm^{-1}	994	1002	985[b]	995
$\nu_{Mo=O,2\leftarrow0}$(IR)/cm^{-1}	1970	1984	1950	1965
$\omega_{Mo=O}$/cm^{-1}	1012	1022	1005	1020
$x_{Mo=O}$	0.009	0.010	0.010	0.012

[a] Fundamental: $\nu_i = \omega_i(1-2x_i)$; first overtone: $\nu_{i,2\leftarrow0} = 2\omega_i(1-3x_i)$ [40].
[b] An additional band at ~1000 cm^{-1} is evidenced for this sample.

observed Raman fundamentals. This is ascribed to anharmonicity, which (at the first place) is the reason for the modification of the vibrational selection rule and for allowing the overtone vibrational transition. By exploiting the wavenumbers of the *observed* Raman $\nu_{Mo=O}$ fundamentals and *observed* IR overtones of $\nu_{Mo=O}$ and by adopting a diatomic approximation we have calculated the zero-order wavenumbers (corrected for anharmonicity), $\omega_{Mo=O}$, as well as the corresponding anharmonic constants. This is done by exploiting the pertinent Raman fundamental ($\nu_{R,Mo=O,1\leftarrow0}$) and IR overtone ($\nu_{IR,Mo=O,2\leftarrow0}$) data and use of the equations:

$$\text{Fundamental}: \ \nu_{Mo=O,\,1\leftarrow0} = \omega_{Mo=O}(1-2x_{Mo=O}) \quad (1)$$

$$\text{First overtone}: \ \nu_{Mo=O,2\leftarrow0} = 2\omega_{Mo=O}(1-3x_{Mo=O}) \quad (2)$$

that relate the *observed* values of the fundamentals and first overtones with the zero-order wavenumber and the anharmonicity constant [40] and the results are listed in Table 2. The calculated anharmonic constant values (~0.01) are very reasonable, thereby qualifying the proposal for mono-oxo configuration.

3.1.3. Vibrational spectra and structural implications

Combined application of Raman and FTIR spectroscopy can provide complementary information on the molecular structure of the dispersed metal oxide phase in supported transition metal oxide catalysts [16]. In particular, one is in principle able to differentiate between e.g. mono-oxo (M=O) and di-oxo [$M(=O)_2$] configuartions. A mono-oxo species will exhibit one single M=O stretching Raman and IR fundamental at (in principle) the same wavenumber in both kinds of spectra, whereas one single overtone may be seen in the IR spectrum. A di-oxo species possesses symmetric ν_s (strong in Raman and weak in IR) and antisymmetric, ν_{as} (weak in Raman and strong in IR) modes the splitting of which lies in the 10–30 cm^{-1} range [40]. Interestingly, the IR overtone region for a di-oxo unit would exhibit multiple features due to overtones and combination bands. However, one should always keep in mind that there exists a very particular case that the symmetric and antisymmetric vibrations of a di-oxo $M(=O)_2$ unit are degenerate and occur at the same wavenumber, namely when the O=M=O angle is 90° [16,41,30].

In the present work, for both systems studied (MoO_3/Al_2O_3 and MoO_3/ZrO_2), at low (1.1–1.7 Mo/nm^2) as well as at high (3.9–5.2 Mo/nm^2) coverage, the observed Raman fundamental, $\nu_{R,1\leftarrow0}$, and IR first overtone, $\nu_{IR,2\leftarrow0}$, constitute (together with the very reasonable anharmonicity constants of ~0.01), a set of values which is consistent with "coinciding" Raman and IR fundamentals at *zero-order wavenumbers* of 1005–1020 cm^{-1} (see Table 2). This is a strong evidence pointing to mono-oxo configurations for the surface MoO_x species on both Al_2O_3 and ZrO_2. One should always remember that the observation of the overtone *per se* precludes the coincidence of the *observed* IR first overtone with the doubled *observed* Raman fundamental.

It is generally adopted as a "rule of thumb" that Mo=O stretching vibrations above 1000 cm^{-1} for molybdena/alumina systems are supportive of the proposal for mono-oxo MoO_x species, based on the vibrational properties (Mo=O modes) of gaseous oxyhalides [40]. However, the prediction of the exact location of Mo=O vibrations for supported MoO_x from data pertaining to gaseous oxyhalides is not straightforward since the halide ligands affect the wavenumber of the oxo-functionalities [12]. Thus, the vibration of a halide-free oxo complex would serve as more accurate reference for supported MoO_x (e.g. 1006 cm^{-1} reported for Keggin $H_3SiM_{12}O_{40}$ clusters that contain mono-oxo Mo=O units [12]). Moreover, recent DFT calculations on MoO_3/Al_2O_3 [42] show that the most abundant species under dehydrated conditions on the most exposed (1 1 0) surface of γ-Al_2O_3 is the mono-oxo O=Mo(–O–Al)$_4$ site with a theoretical Mo=O stretching frequency of 1015 cm^{-1} in full agreement with the primary wavenumbers, $\omega_{Mo=O}$, listed in Table 2 (2nd and 3rd column). Notably, the same calculations for the *much less abundant* di-oxo species on the minor (100) facet of γ-Al_2O_3 predict ν_s/ν_{as} pairs at 980/960 cm^{-1}, far below the observed single Raman wavenumbers (~1000 cm^{-1}) and the zero-order wavenumbers (~1015 cm^{-1}). Therefore, the proposal for mono-oxo configuration for MoO_x on Al_2O_3 is further justified.

3.2. In situ Raman spectra and $^{18}O/^{16}O$ isotope exchange

3.2.1. Introductory remarks

The study of metal–oxygen vibrations of a transition metal oxide phase which is dispersed on a support oxide is of great importance since it can provide valuable information on structural and configurational aspects of the deposited sites in catalytic materials. *In situ* vibrational (Raman and IR) spectroscopies combined with ^{18}O isotopic labelling studies can e.g. lead to differentiation between mono-oxo M=O, di-oxo $M(=O)_2$ or tri-oxo $M(=O)_3$ configurations and the relevant systematics are well-known and have been elegantly summarised in e.g. Ref. [43]. Very briefly (with relevance to combined *in situ* Raman and ^{18}O isotopic labelling [30]) a M=O species will exhibit two Raman bands (due to M=^{16}O and M=^{18}O), a di-oxo $M(=O)_2$ species will exhibit three Raman bands (due to ^{16}O=M=^{16}O, ^{16}O=M=^{18}O and ^{18}O=M=^{18}O), whereas a tri-oxo $M(=O)_3$ species should give rise to four Raman bands (due to $M(=^{16}O)_3$, ^{18}O=$M(=^{16}O)_2$, $(^{18}O)_2$=M=^{16}O and $(^{18}O)_3$=M) [40].

The theory of vibrational isotope effects in polyatomic molecules is quite elaborate and has been well documented long time ago [44]. The situation becomes much simpler if the diatomic approximation can be adopted, like e.g. in the case of a mono-oxo M=O configuration of a dispersed metal oxide phase. On the basis of equal interatomic M–O distance between the M=^{16}O and M=^{18}O counterparts it can easily be shown that the isotopic ratio, defined as the $\nu_{M=^{16}O}/\nu_{M=^{18}O}$ ratio is equal to [40]:

$$\text{isotopic ratio}: \ \frac{\nu_{M=^{16}O}}{\nu_{M=^{18}O}} = \frac{\sqrt{(1/m_M)+(1/m_{^{16}O})}}{\sqrt{(1/m_M)+(1/m_{^{18}O})}} \quad (3)$$

where m_i are the respective atomic masses. For the case of Mo–O diatomic oscillator the isotopic ratio is equal to 1.0513.

3.2.2. Spectra of the MoO_3–Al_2O_3 catalytic system

Fig. 5 shows sequential snapshots of intermittent *in situ* Raman spectra obtained at 450 °C for the 5MoAl (1.1 Mo/nm^2) catalyst after successive reduction/oxidation cycles (with 4.5% H_2/N_2 and

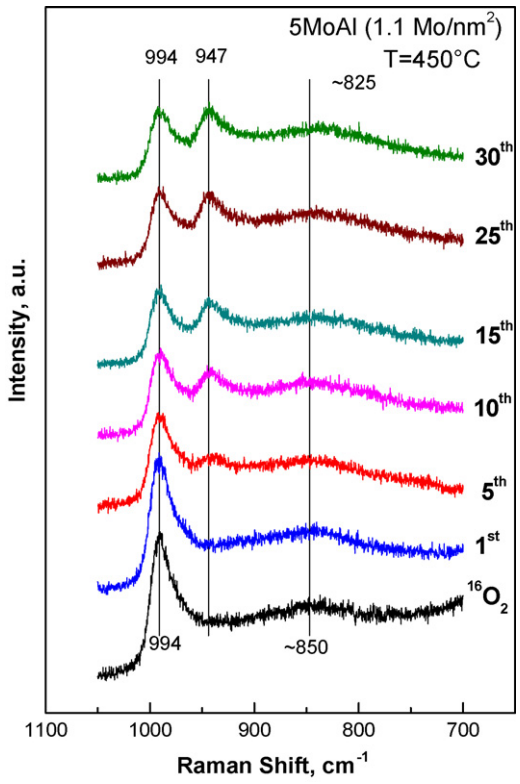

Fig. 5. *In situ* sequential Raman spectra obtained for the 5MoAl sample at 450 °C under flowing 2% $^{18}O_2$/He after reduction(H_2)/oxidation($^{18}O_2$) cycles as indicated by each spectrum. Recording parameters: see Fig. 2 caption.

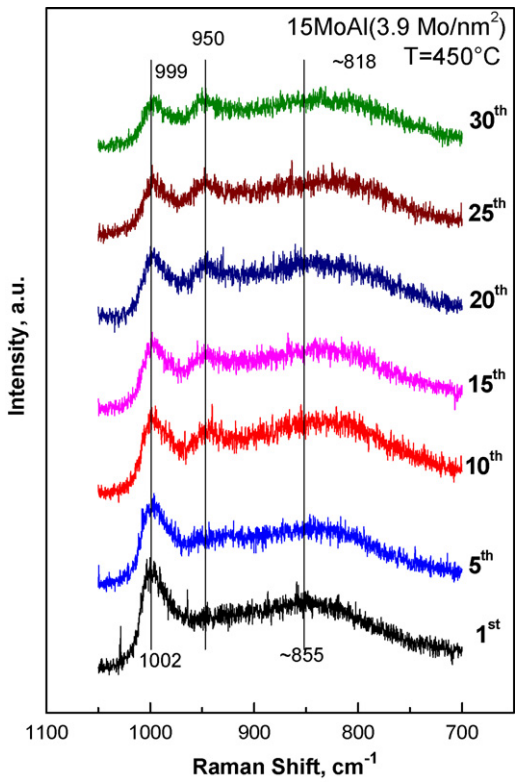

Fig. 6. *In situ* sequential Raman spectra obtained for the 15MoAl sample at 450 °C under flowing 2% $^{18}O_2$/He after reduction (H_2)/oxidation ($^{18}O_2$) cycles as indicated by each spectrum. Recording parameters: see Fig. 2 caption.

2% $^{18}O_2$/He, respectively) as indicated by each spectrum. Fig. 6 illustrates the respective series of spectra obtained for the 15MoAl (3.9 Mo/nm^2) catalyst. The following observations are made:

(i) The bands due to Mo=^{16}O (observed at 994 cm^{-1} for 5MoAl (Fig. 5) and at 1002 cm^{-1} for 15MoAl (Fig. 6)) progressively loose intensity and new bands appear (observed at 947 cm^{-1} for 5MoAl (Fig. 5) and at 950 cm^{-1} for 15MoAl (Fig. 6)) which can be assigned to Mo=^{18}O and progressively gain intensity as a function of reduction/oxidation cycles, indicating a progress in ^{18}O/^{16}O exchange;
(ii) only one new band appears for each catalyst in the M=O stretching region;
(iii) almost 90% of the progress achieved after 30 reduction/oxidation cycles in ^{18}O/^{16}O exchange is reached after 15–20 reduction/oxidation cycles under the applied conditions;
(iv) the bands due to Mo–O–Mo functionalities (observed at ~850 cm^{-1} for 5MoAl (Fig. 5) and at ~855 cm^{-1} for 15MoAl (Fig. 6)) are progressively shifted to ~825 cm^{-1} for 5MoAl (Fig. 5) and at ~818 cm^{-1} for 15MoAl (Fig. 6); and
(v) the *final* (after 30 reduction/oxidation cycles for ^{18}O/^{16}O exchange) position of the Mo=^{16}O band remains *unchanged* (994 cm^{-1}) for the low-loaded 5MoAl (Fig. 5) but is slightly *red-shifted* (from 1002 to 999 cm^{-1}) for the high-loaded 15MoAl (Fig. 6).

All pertinent information on band wavenumbers as well as the theoretically expected band positions (calculated using the isotopic ratio 1.0513) are listed in Table 3.

3.2.3. Spectra of the MoO_3–ZrO_2 catalytic system

Figs. 7 and 8 show the sequential snapshots of intermittent *in situ* Raman spectra obtained at 450 °C for the 2MoZr (1.7 Mo/nm^2) and for the 5.5MoZr (5.2 Mo/nm^2) catalysts, respectively after successive reduction/oxidation cycles (with 4.5% H_2/N_2 and 2% $^{18}O_2$/He, respectively) as indicated by each spectrum. After completion of the sequential reduction/oxidation cycles, the recording of the last spectrum was repeated with higher resolution, in view of the fact that MoO_3–ZrO_2 catalysts exhibit two distinct peaks in the Mo=O terminal stretching region [5] (see also the discussion pertain-

Table 3
Vibrational isotope effects for MoO_3/Al_2O_3 and MoO_3/ZrO_2 catalysts. observed and theoretically calculated Raman band wavenumbers (Figs. 5–8).

Catalyst sample	Mo=^{16}O[a]	Mo=^{18}O		Mo=^{16}O[b]	Mo–^{16}O–Mo [a]	Mo–^{18}O–Mo	
(Mo/nm^2)	(Raman)	(Raman)[b]	(calculated)[c]	(Raman)	(Raman)	(Raman)[b]	(calculated)[c]
5MoAl (1.1)	994	947	945	994	850	825	809
15MoAl (3.9)	1002	950	953	999	855	818	813
2MoZr (1.7)	985	936	937	983	837	810	796
5.5MoZr (5.2)	995	943	946	990	851	817	809

[a] Before ^{18}O/^{16}O exchange.
[b] Final position of band after 30 reduction/oxidation cycles of ^{18}O/^{16}O exchange.
[c] Based on the isotopic ratio: 1.0513.

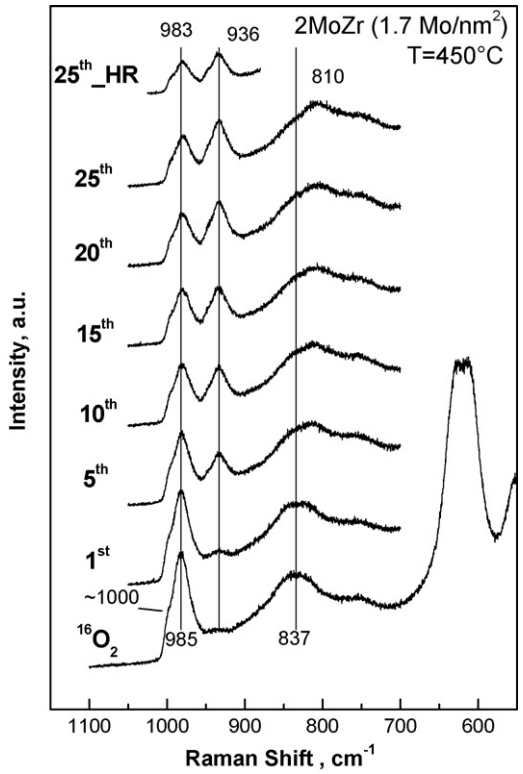

Fig. 7. *In situ* sequential Raman spectra obtained for the 2MoZr sample at 450 °C under flowing 2% $^{18}O_2$/He after reduction (H_2)/oxidation ($^{18}O_2$) cycles as indicated by each spectrum. Recording parameters: see Fig. 2 caption, except for the high resolution spectrum (HR) obtained with spectral slit width, ssw = 3 cm^{-1}.

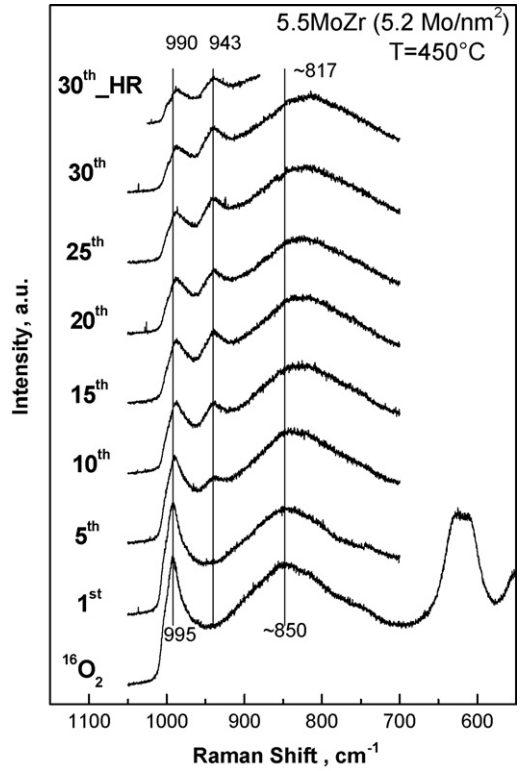

Fig. 8. *In situ* sequential Raman spectra obtained for the 5.5MoZr sample at 450 °C under flowing 2% $^{18}O_2$/He after reduction (H_2)/oxidation ($^{18}O_2$) cycles as indicated by each spectrum. Recording parameters: see Fig. 2 caption, except for the high resolution spectrum (HR) obtained with spectral slit width, ssw = 3 cm^{-1}.

ing to the context of Fig. 3). The following observations are made:

(i) The main bands due to Mo=^{16}O (observed at 985 cm^{-1} for 2MoZr (Fig. 7) and at 995 cm^{-1} for 5.5MoZr (Fig. 8)) progressively loose intensity and new bands appear (observed at 936 cm^{-1} for 2MoZr (Fig. 7) and at 943 cm^{-1} for 5.5MoZr (Fig. 8)) which can be assigned to Mo=^{18}O and progressively gain intensity as a function of reduction/oxidation cycles, indicating a progress in $^{18}O/^{16}O$ exchange;

(ii) the band "pattern" of the newly emerging band is identical to the initial Mo=^{16}O band in each case (Figs. 7 and 8), *i.e.* it possesses a high frequency shoulder which is better resolved for the low-loaded sample (Fig. 7) for which the main band is located 7–10 cm^{-1} lower compared to the high-loaded sample (e.g. 936 cm^{-1} vs. 943 cm^{-1} for Mo=^{18}O and 985 cm^{-1} vs. 995 cm^{-1} for Mo=^{16}O);

(iii) more than 90% of the progress achieved after 30 reduction/oxidation cycles in $^{18}O/^{16}O$ exchange is reached after 20 reduction/oxidation cycles under the applied conditions;

(iv) the bands due to Mo–O–Mo functionalities (observed at 837 cm^{-1} for 2MoZr (Fig. 7) and at ~850 cm^{-1} for 5.5MoZr (Fig. 8)) are progressively shifted to 810 cm^{-1} for 2MoZr (Fig. 7) and to ~817 cm^{-1} for 5.5MoZr (Fig. 8); and

(v) the *final* (after 25 or 30 reduction/oxidation cycles for $^{18}O/^{16}O$ exchange) position of the Mo=^{16}O bands are slightly *red-shifted* to an extent which is higher for the high-loaded sample (from 985 to 983 cm^{-1} for the low-loaded 2MoZr (Fig. 7) and from 995 to 990 cm^{-1} for the high-loaded 5.5MoZr (Fig. 8)).

The observed band wavenumbers as well as the theoretically expected band positions (calculated using the isotopic ratio 1.0513) are also listed in Table 3.

3.2.4. Vibrational isotope effects, interpretations and structural implications

All observations made in the present work point to a mono-oxo configuration of the dispersed molybdena phase on Al_2O_3 and ZrO_2 both at low (1.1–1.7 Mo/nm^2) as well as at high coverage (3.9–5.2 Mo/nm^2). The same conclusion has earlier been reached for a high-loaded MoO_3/ZrO_2 catalyst by *in situ* Raman spectra combined with $^{18}O/^{16}O$ exchange [30] and the strategy applied in that work is adopted also in the present work to a large extent. The present proposal for the mono-oxo configuration which is based on the indications provided from the study of the vibrational isotope effects builds on the evidence found in the combined *in situ* Raman and FTIR spectra (*vide ante*). Below, we discuss the various structural implications and interpretations at the molecular level.

The first indication of the $^{18}O/^{16}O$ isotope exchange pointing to mono-oxo configuration comes from a close examination of Figs. 5–8, showing that the isotopic substitution follows the scenario of two bands being present in the Mo=O stretching region (*i.e.* due to Mo=^{16}O and Mo=^{18}O) during the sequential $^{18}O/^{16}O$ isotope exchange. The second indication comes from the corroboration of the hypothesis for the existence of a diatomic unit containing terminal oxygen (Mo=O) which enables a theoretical prediction of the isotopic effect on the vibrational wavenumber based on the isotopic ratio 1.0513. This is best seen in Table 3, where the observed Mo=^{18}O wavenumbers are in excellent agreement with those theoretically predicted. The agreement is less shining for the isotope effect on Mo–O–Mo functionalities, but this is obviously ascribed to a suffering of the diatomic approach for the bridging unit.

It is worth mentioning that as stated above in Section 3.1.3 describing the structural implications of the *in situ* vibrational spectra there is one single possibility for a di-oxo unit to exhibit one

single band in the Raman spectrum due to degeneration effects, if the angle within the O=Mo=O bond is 90° and the force constants of the independent Mo–O bonds are the same. However, it is extremely unlikely (given also the molybdena site multiplicity) that this could occur in low as well as high loadings in both catalytic systems studied in this work.

Finally, we address the small shifts of the Mo=^{16}O Raman band, *i.e.* the occasional difference between the initial (before isotopic exchange) and the final (after completion of the reduction/oxidation cycles resulting in ^{18}O/^{16}O exchange) position of the Mo=^{16}O band (see Table 3). It is worth to note that in Figs. 7 and 8 (pertaining to MoO_3–ZrO_2 catalysts) where the signal-to-noise ratio is much higher, the shift in the Mo=^{16}O band wavenumber is already clear after the 10th cycle. This effect is ascribed to a perturbation in bond length (elongation) and strength (weakening) of the Mo=^{16}O bond caused by the ^{18}O/^{16}O exchange of O sites which are next-nearest-neighbors to the terminal ^{16}O of the Mo=^{16}O bond. Such oxygen sites can belong either to Mo–^{18}O–Mo′ units bridging to other Mo atom (denoted Mo′) in associated (polymeric) units or to Mo–^{18}O–*S* (*S* = support metal atom) anchoring bridges. The effective nuclear charge of the ^{18}O is lower due to the higher number of neutrons, thereby resulting in a slightly lower electronegativity for the ^{18}O atom in Mo–^{18}O–Mo′ and/or Mo–^{18}O–*S* bridges (should an ^{18}O/^{16}O exchange had taken place within these units). In turn, a slightly higher basicity (electron donating ability) is resulted for the ^{18}O atom and thereby a slight strengthening of the Mo–^{18}O(–Mo′) and/or Mo–^{18}O(–*S*) bonds takes place. Such an effect will cause a slight weakening of the Mo=^{16}O terminal bond and a slight *red shift* of its wavenumber, by that means explaining the observed shifts in the respective Mo=^{16}O band wavenumbers (Table 3). However, in one case (5MoAl) the Mo=^{16}O band remains at the *same wavenumber* after 30 reduction oxidation cycles of ^{18}O/^{16}O exchange (994 cm^{-1}, Fig. 5), while in all three other samples *red shifts* are observed. For the low-loaded 5MoAl sample, an inspection of Figs. 2 and 5 shows that the ~850 cm^{-1} band due to Mo–O–Mo functionalities is very weak, therefore isolated monomolybdates dominate within the deposited molybdena phase and (effectively) there are very few O atoms bridging between Mo atoms. Furthermore, it is known that the alumina support is hardly reducible [45], thus for the 5MoAl sample the aforementioned ^{18}O/^{16}O exchange of O atoms which are next-nearest-neighbor to the ^{16}O of the Mo=^{16}O unit does *not* take place from an effective point of view and the 994 cm^{-1} Mo=^{16}O band does *not* shift after 30 cycles of ^{18}O/^{16}O exchange (Fig. 5). To the contrary, the gradual ^{18}O/^{16}O exchange of the ^{16}O atoms within Mo–O–Mo bridges (Mo–^{16}O–Mo′ → Mo–^{18}O–Mo′) results in red shifts of the terminal Mo=^{16}O bands for 15MoAl (Fig. 6), 2MoZr (Fig. 7) and 5.5MoZr (Fig. 8) to an extent which is apparently proportional to the extent of the polymolybdate presence (evidence by the occurrence and intensity of the Mo–O–Mo band).

We proceed by illustrating that the Mo–^{16}O–Mo′ → Mo–^{18}O–Mo′ substitution is the only one taking place also in the case of MoO_3–ZrO_2 catalysts, as far as the oxygen next-nearest-neigbors to the ^{16}O of the Mo=^{16}O are concerned. Fig. 9 shows the *in situ* Raman spectra obtained at 450 °C for the 5.5MoZr catalyst under flowing $^{16}O_2$ and after 10 reduction/oxidation cycles of ^{18}O/^{16}O exchange under flowing 2% $^{18}O_2$/He. The isotope effects (appearance of bands due to Mo=^{18}O and Mo–^{18}O–Mo′) and the newly reported effect of the "next-nearest-neighbor ^{18}O/^{16}O substitution" which results in a red shift of the Mo=^{16}O band are clearly observed, while all bands due to the monoclinic ZrO_2 support remain unshifted, thereby indicating that under the applied conditions the zirconia support is hardly reducible. Unfortunately, no such confirmation can be done for alumina, due to lack of well-defined Raman bands.

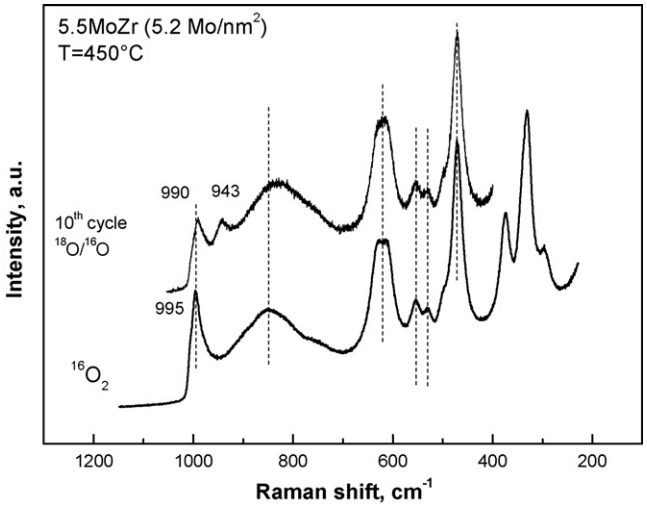

Fig. 9. *In situ* Raman spectra obtained for the 5.5MoZr sample at 450 °C under flowing $^{16}O_2$ (bottom) and 2% $^{18}O_2$/He after 10 reduction (H_2)/oxidation ($^{18}O_2$) cycles (top). Recording parameters: see Fig. 2 caption.

3.3. Catalyst behavior for the ODH of ethane

Detailed catalytic studies of MoO_3/Al_2O_3 and MoO_3/ZrO_2 catalysts for the ODH of ethane have been addressed separately [5,8] and were beyond the scope of the present work. We hereby append highlights of the catalytic performance in order to address certain structure/activity relations.

Fig. 10 shows the dependence of ethylene selectivity on various levels of ethane conversion, achieved by varying the residence time, expressed by the *W*/*F* ratio, for the studied catalysts at 540 °C. A slight decrease in selectivity is observed with increasing conversion for the MoAl samples, while the selectivity of MoZr samples exhibit a remarkable stability, even at high conversions. The slight decrease in ethylene selectivity with increasing conversion is due to secondary combustion reactions of ethylene to CO_x. Initial (*i.e.* at nearly zero conversion) non-selective reaction pathways can be evidenced for the MoZr samples and probably for 5MoAl, by extrapolation of the curves. It should be noted that ethylene selectivity is lower at low surface MoO_x coverage, due to direct (via non-selective pathway) reaction with the unselective exposed support sites [5,8].

Comparative assessments of catalyst activity can be made on the basis of TOF (turnover frequency, *i.e.* ethane conversion or ethylene

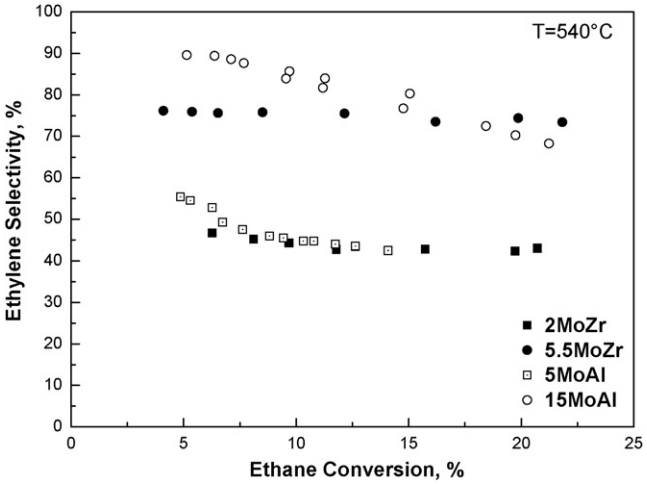

Fig. 10. Ethylene selectivity as a function of ethane conversion. *T* = 540 °C.

Table 4
Initial apparent TOFs of ethane consumption and ethylene production for low-loaded and high-loaded MoO_3/Al_2O_3 and MoO_3/ZrO_2 catalysts. $W/F = 0.28\,g\,s/cm^3$; $T = 540\,^{\circ}C$.

Catalyst	Mo surface density (Mo/nm^2)	Apparent ethane consumption TOF [mol/(Mo s)]	Apparent ethylene production TOF [mol/(Mo s)]
5MoAl	1.1	2.8×10^{-3}	1.4×10^{-3}
15MoAl	3.9	2.6×10^{-3}	1.8×10^{-3}
2MoZr	1.7	20.0×10^{-3}	8.5×10^{-3}
5.5MoZr	5.2	5.9×10^{-3}	4.2×10^{-3}

production rates expressed per Mo atom). Ideally, TOFs have to be expressed per active Mo only; however this is not possible even if dispersion data were available, because not all surface Mo atoms are active (see Section 1). Therefore, we adopt the term *apparent* TOF to account for the above. Table 4 lists the pertinent TOF data for the studied catalysts. In all cases it appears that MoO_3/ZrO_2 perform better compared to MoO_3/Al_2O_3 catalysts, despite the fact that the structural and configurational characteristics are quite common amongst the two sets of materials, as evidenced in the preceding sub-sections. An exception holds for the relative distribution of monomeric vs. polymeric molybdates, namely a higher relative occurrence in the form of polymolybdates on the zirconia support. The support effect in selective oxidation reactions (including *inter-alia* the ODH of light alkanes) appears to have a stronger influence when compared to the effect of surface MoO_x coverage (see Table 4). In particular the support effect has been addressed repeatedly in the literature [24,35,46–51] pointing to the importance of Mo–O-support bonds for the catalytically relevant step. Notably, an inverse correlation between the steady-state TOF and the support cation electronegativity underlines the support effect quiet demonstratively [24,49–51]. Furthermore, the participation of lattice oxygen atoms in reactive intermediates during light alkane ODH reactions over supported metal oxides has been evidenced by isotopic labelling studies [52,53]. In ODH reactions over supported metal oxides, the rate-limiting step is a redox process involving C–H bond cleavage [54,55]. The proposed Mars-van Krevelen mechanism decouples the oxidation of the reactant from the reoxidation of the catalyst. Finally it is worth mentioning that the data in Table 4 show that the apparent TOF values for ethylene production are almost insensitive to surface coverage and to the nuclearity (*i.e.* monomeric vs. polymeric form) of the deposited $(MoO_x)_n$. This is more striking for MoO_3/Al_2O_3 system for which although the Raman results point to an almost exclusive existence of monomers at low coverage (1.1 Mo/nm^2) with polymeric units prevailing at 3.9 Mo/nm^2, the ethylene TOF's are 1.4×10^{-3} and 1.8×10^{-3} mol/(Mos), respectively. Therefore, surface $(MoO_x)_n$ in monomeric as well as polymeric form appear catalytically active for the ethane ODH reaction. At monolayer coverage, a heterogeneity of the active phase may prevail, with isolated and polymeric species both acting as reactive sites.

Another important issue pertains to the effect of surface acidity on ethane ODH reaction. For MoO_3/Al_2O_3 catalysts, it is known that there is no Bronsted acidity at low coverage [56], whereas Bronsted acid sites are present at high coverage, below monolayer [56]. Thus, the monomeric units that (as judged by the Raman results) predominate on the 5MoAl (1.1 Mo/nm^2) sample do not possess Bronsted acidity, but the polymeric species present on 15MoAl (3.9 Mo nm^2) possess Bronsted acidity. Naturally, both monomeric and polymeric units are present at 3.9 Mo/nm^2 but the appearance of Bronsted acidity has previously been ascribed to the presence of polymeric units [56]. Interestingly, the apparent ethylene TOF values (Table 4) are the same for the two samples despite the lack of Bronsted acid sites on the low-loaded sample.

However, as pointed out in Section 1, the structural and configurational properties are not adequate for assuring a "good catalyst function". Aspects related to favorable balance between oxygen site reducibility, acid–base characteristics, oxygen mobility, lattice diffusivity, support effects, etc. are of key importance for a functional catalyst.

4. Conclusions

In situ vibrational (Raman and FTIR) spectroscopy was used for studying the molecular structure and configuration of the deposited molybdena phase of catalysts supported on alumina and zirconia. *In situ* Raman spectroscopy was applied in combination with $^{18}O/^{16}O$ isotope exchange studies. The vibrational isotope effects and the combined interpretation of Raman and IR band wavenumbers and characteristics point to a mono-oxo configuration for the deposited molybdena phase at low (1.1–1.7 Mo/nm^2) as well as at high (3.9–5.2 Mo/nm^2) coverage on both supports irrespective of polymerisation degree (*i.e.* for isolated monomolybdates and associated/polymeric molybdates). Deposited molybdena occurs predominantly in the form of mono-oxo monomolybdates on alumina at low coverage (1.1 Mo/nm^2), while mono-oxo polymolybdates accumulate at higher loadings. Mono-oxo polymolybdates and monomolybdates occur on zirconia, with the polymolybdates predominating already from low coverage (1.7 Mo/nm^2). A "next-nearest-neighbor $^{18}O/^{16}O$ substitution" effect is observed which results in a red shift (2–5 cm^{-1}) of the Mo=^{16}O band. This effect takes place upon substitution of oxygen atoms which are next-nearest-neighbors to the terminal ^{16}O. Such an isotopic substitution can selectively take place before the substitution of the terminal ^{16}O. The catalytic data show that the nuclearity (e.g. monomer or polymer) is not critical for the catalytic activity of deposited $(MoO_x)_n$ units for the ethane ODH reaction. Variations in the catalytic performance of MoO_3/Al_2O_3 and MoO_3/ZrO_2 catalysts for the ODH of ethane cannot be accounted for exclusively on the basis of structural/configurational similarities and variations. Factors such as the support effect (e.g. electronegativity of support cation) appear to be of key importance.

Acknowledgement

Financial support was provided by the Research Committee of the University of Patras (C. Caratheodory program C.583).

References

[1] J. Handzlik, J. Phys. Chem. B 109 (2005) 20794.
[2] J.M. Jehng, H.C. Hu, X.T. Gao, I.E. Wachs, Catal. Today 28 (1996) 335.
[3] H.C. Liu, E. Iglesia, J. Catal. 208 (2002) 1.
[4] K.D. Chen, A.T. Bell, E. Iglesia, J. Catal. 209 (2002) 35.
[5] A. Christodoulakis, S. Boghosian, J. Catal. 260 (2008) 178.
[6] I. Nova, L. Lietti, L. Casagrande, L. Dall'Acqua, E. Giamello, P. Forzatti, Appl. Catal. B 17 (1998) 245.
[7] G. Mestl, T.K.K. Srinivasan, Catal. Rev. Sci. Eng. 40 (4) (1998) 451.
[8] A. Christodoulakis, E. Heracleous, A.A. Lemonidou, S. Boghosian, J. Catal. 242 (2006) 16.
[9] S. Xie, K. Chen, A.T. Bell, E. Iglesia, J. Phys. Chem. B 104 (2000) 10059.
[10] S. Chempath, Y. Zhang, A.T. Bell, J. Phys. Chem. C 111 (2007) 1291.
[11] K. Hamraoui, S. Cristol, E. Payen, J.-F. Paul, J. Phys. Chem. C 111 (2007) 3963.
[12] E.L. Lee, I.E. Wachs, J. Phys. Chem. C 111 (2007) 14410.
[13] E.L. Lee, I.E. Wachs, J. Phys. Chem. C 112 (2008) 6487.
[14] I.E. Wachs, Catal. Today 27 (1996) 437.
[15] G. Mestl, J. Mol. Catal. A: Chem. 158 (2000) 45.
[16] G. Busca, J. Raman Spectrosc 33 (2002) 348.
[17] M.A. Banares, I.E. Wachs, J. Raman Spectrosc. 33 (2002) 359.
[18] Operando Spectroscopy: fundamental and technical aspects of spectroscopy of catalysts under working conditions, Phys. Chem. Chem. Phys. 5 (Special issue (20)) (2003).
[19] B.M. Weckhuysen, Chem. Commun. (2002) 97.
[20] C.G. Cortez, M.A. Banares, J. Catal. 209 (2002) 197.
[21] A.M. Beale, A.M.J. van der Eerden, K. Kervinen, M.A. Newton, B.M. Weckhuysen, Chem. Commun. (2005) 3015.

[22] B.M. Weckhuysen, Angew. Chem. 48 (2009) 4910.
[23] H. Hu, I.E. Wachs, S.R. Bare, J. Phys. Chem. 99 (1995) 10897.
[24] G. Tsilomelekis, A. Christodoulakis, S. Boghosian, Catal. Today 127 (2007) 139.
[25] R. Radhakrishnan, C. Reed, S.T. Oyama, M. Senman, J.N. Kondo, K. Domen, Y. Ohminami, K. Asakura, J. Phys. Chem. B 105 (2001) 8519.
[26] M. Vuurman, I.E. Wachs, J. Phys. Chem. 96 (1992) 5008.
[27] H.C. Liu, P. Cheung, E. Iglesia, J. Catal. 217 (2003) 222.
[28] K. Chen, S. Xie, E. Iglesia, A.T. Bell, J. Catal. 189 (2000) 421.
[29] H. Dai, A.T. Bell, E. Iglesia, J. Catal. 221 (2004) 491.
[30] B.M. Weckhuysen, J.-M. Jehng, I.E. Wachs, J. Phys. Chem. B 104 (2000) 7382.
[31] L.J. Burcham, J. Datka, I.E. Wachs, J. Phys. Chem. B 103 (1999) 6015.
[32] D.S. Kim, M. Ostromecki, I.E. Wachs, J. Mol. Catal. A: Chem. 106 (1996) 93.
[33] I.E. Wachs, Top. Catal. 8 (1999) 57.
[34] H. Knozinger, G. Mestl, Top. Catal. 8 (1999) 45.
[35] D.S. Kim, I.E. Wachs, K. Segawa, J. Catal 146 (1994) 268.
[36] E. Payen, S. Lasztelan, J. Grimblot, J.P. Bonelle, J. Raman Spectrosc. 17 (1986) 233.
[37] R.B. Watson, U.S. Ozkan, J. Catal. 208 (2002) 124.
[38] N. Magg, B. Immaraporn, J.B. Giorgi, T. Schroeder, M. Baumer, J. Dobler, Z. Wu, E. Kondratenko, M. Cherian, M. Baerns, P.C. Stair, J. Sauer, H.-J. Freund, J. Catal. 226 (2004) 88.
[39] V. Bradzova, M.V. Ganduglia-Pirovano, J. Sauer, J. Phys. Chem. C 114 (2010) 4983.
[40] K. Nakamoto, Infrared and Raman Spectra of Inorganic and Coordination Compounds, 6th ed., Wiley–Interscience, New York, 2009.
[41] A.B.P. Lever, Inorganic Electronic Spectroscopy, Elsevier, New York, 1968.
[42] J. Handzlik, P. Sautet, J. Phys. Chem. C 112 (2008) 14456.
[43] B.M. Weckhuysen, I.E. Wachs, J. Phys. Chem. B 101 (1997) 2793.
[44] E.O. Salant, J.E. Rosenthal, Phys. Rev. 42 (1932) 812.
[45] A. Lycourghiotis, private communication.
[46] B.M. Weckhuysen, D.E. Keller, Catal. Today 78 (2003) 25.
[47] E. Heracleous, M. Machli, A.A. Lemonidou, I.A. Vasalos, J. Mol. Catal. A: Chem. 232 (2005) 29.
[48] M. Banares, G. Mestl, Advances in Catalysis, vol. 52, Elsevier, 2009, p. 43.
[49] I.E. Wachs, Catal. Today 100 (2005) 79.
[50] C. Zhao, I.E. Wachs, J. Catal. 257 (2008) 181.
[51] E.L. Lee, I.E. Wachs, in: U. Ozkan (Ed.), Design of Heterogeneous Catalysts: New Approaches based on Synthesis, Characterization and Modeling, Wiley-VCH, Weinheim, 2009, p. 1.
[52] K. Chen, A. Khodakov, J. Yang, A.T. Bell, E. Iglesia, J. Catal. 186 (1999) 325.
[53] K. Chen, E. Iglesia, A.T. Bell, J. Catal. 192 (2000) 197.
[54] M.D. Argyle, K. Chen, A.T. Bell, E. Iglesia, J. Phys. Chem. B 106 (2002) 5421.
[55] B. Kilos, A.T. Bell, E. Iglesia, J. Phys. Chem. C 113 (2009) 2830.
[56] A.M. Turek, I.E. Wachs, J. Phys. Chem. 96 (1992) 5000.